Dynamics of intrinsic axial flows in unsheared, uniform magnetic fields

J. C. Li, P. H. Diamond, X. Q. Xu, and G. R. Tynan

Citation: Physics of Plasmas **23**, 052311 (2016); doi: 10.1063/1.4950830
View online: http://dx.doi.org/10.1063/1.4950830
View Table of Contents: http://scitation.aip.org/content/aip/journal/pop/23/5?ver=pdfcov
Published by the AIP Publishing

Dynamics of intrinsic axial flows in unsheared, uniform magnetic fields

J. C. Li,[1] P. H. Diamond,[1] X. Q. Xu,[2] and G. R. Tynan[3,1]
[1]CMTFO and CASS, University of California, San Diego, California 92093, USA
[2]Lawrence Livermore National Laboratory, Livermore, California 94550, USA
[3]Center for Energy Research and Department of Mechanical and Aerospace Engineering, University of California at San Diego, San Diego, California 92093, USA

(Received 1 March 2016; accepted 3 May 2016; published online 27 May 2016)

A simple model for the generation and amplification of intrinsic axial flow in a linear device, controlled shear decorrelation experiment, is proposed. This model proposes and builds upon a novel dynamical symmetry breaking mechanism, using a simple theory of drift wave turbulence in the presence of axial flow shear. This mechanism does not require complex magnetic field structure, such as shear, and thus is also applicable to intrinsic rotation generation in tokamaks at weak or zero magnetic shear, as well as to linear devices. This mechanism is essentially the self-amplification of the mean axial flow profile, i.e., a modulational instability. Hence, the flow development is a form of negative viscosity phenomenon. Unlike conventional mechanisms where the residual stress produces an intrinsic torque, in this dynamical symmetry breaking scheme, the residual stress induces a negative increment to the ambient turbulent viscosity. The axial flow shear is then amplified by this negative viscosity increment. The resulting mean axial flow profile is calculated and discussed by analogy with the problem of turbulent pipe flow. For tokamaks, the negative viscosity is not needed to generate intrinsic rotation. However, toroidal rotation profile gradient is enhanced by the negative increment in turbulent viscosity. *Published by AIP Publishing.*
[http://dx.doi.org/10.1063/1.4950830]

I. INTRODUCTION

Toroidal rotation of plasma is beneficial to both macrostability, e.g., the mitigation or stabilization of resistive wall modes,[1] and microstability, by suppressing turbulence via toroidal shear flows that contribute to $E \times B$ shear flows. Plasma rotation and the underlying toroidal angular momentum transport were intensively first studied because neutral beam injection (NBI) was the heating method of choice for tokamaks. Given the fact that unbalanced NBI naturally drives toroidal rotation, and along with the experimental observation that the ion momentum and thermal diffusivities were comparable ($\chi_\phi \sim \chi_i$),[2] toroidal momentum transport was thought to be diffusive and comparable to the ion heat transport. However, the discovery of the non-diffusive character of toroidal momentum transport in the JFT-2M tokamak[3] disrupted that overly simple understanding of the toroidal rotation. The paradigm shift was finally triggered by the observation of intrinsic core rotation in the Alcator-C-Mod tokamak, for both Ohmically heated and ion cyclotron resonance frequency driven plasma discharges.[4,5] Here, intrinsic rotation means plasma rotation without NBI drives or external wave momentum torque, i.e., self-accelerated rotation. Given the benefits of plasma rotations, the intrinsic rotation is particularly favorable for the International Thermonuclear Experimental Reactor (ITER), where NBI driven rotation is not feasible.

The discovery of intrinsic rotation has elicited interest in the nondiffusive flux (pinch and residual stress) of toroidal momentum which can accelerate the central plasma rotation.[6] The momentum pinch, which redistributes the toroidal momentum, contributes little to rotation generation.[7,8] Hence, the Reynolds stress has the generic form

$$\langle \tilde{v}_r \tilde{v}_\phi \rangle \cong -\chi_\phi \frac{\partial \langle v_\phi \rangle}{\partial r} + \Pi^{\mathrm{Res}}_{r\phi}. \tag{1}$$

The residual stress is driven by the background turbulence, i.e., $\Pi^{\mathrm{Res}}_{r\phi} = \Pi^{\mathrm{Res}}_{r\phi}(\nabla n_0, \nabla T_{i,e})$, and can accelerate the plasma from rest via the intrinsic torque $\tau = -\partial_r \Pi^{\mathrm{Res}}_{r\phi}$. The process that the profile gradients drive intrinsic rotations via the residual stress is analogous to a car engine which converts heat flux into the motion of wheels.[9] $\Pi^{\mathrm{Res}}_{r\phi}$ is also a counterpart of the poloidal residual stress that accelerates poloidal flow.[10] The turbulent diffusion of toroidal momentum is also driven by the ambient background turbulence, i.e., $\chi_\phi = \chi_\phi(\nabla n_0, \nabla T_{i,e})$. Thus, as a result of the balance between $\Pi^{\mathrm{Res}}_{r\phi}$ and χ_ϕ, the rotation profile steepens as a secondary effect of the free energy sources (∇n_0, $\nabla T_{i,e}$). If the rotation profile steepens enough to drive a tertiary instability, i.e., parallel shear flow instability (PSFI),[11,12] then $\nabla\langle v_\parallel \rangle$ will act as an additional drive for the turbulent viscosity, i.e., $\chi_\phi = \chi_{\phi,1}(\nabla n_0, \nabla T_{i,e}) + \chi^{\mathrm{PSFI}}_\phi(\nabla\langle v_\parallel \rangle)$. As a consequence, the intrinsic rotation profile is relaxed by the additional viscosity driven by $\nabla\langle v_\parallel \rangle$ because $\langle v_\phi \rangle' \sim \Pi^{\mathrm{Res}}_{r\phi}/(\chi_{\phi,1} + \chi^{\mathrm{PSFI}}_\phi)$. This is somewhat analogous to the zonal flow saturation by tertiary instability (Fig. 1).[13]

Usually, the toroidal rotation is driven by the parallel residual stress $\Pi^{\mathrm{Res}}_{r\parallel}$ that emerges from $\langle \tilde{v}_r \tilde{v}_\parallel \rangle$. $\Pi^{\mathrm{Res}}_{r\parallel}$ is determined by the spectral correlator $\langle k_\theta k_\parallel \rangle \equiv \sum_k k_\theta k_\parallel |\phi_k|^2$ which requires symmetry breaking, i.e., spectral imbalance in $\mathbf{k}$ space.[14–16] Conventional mechanisms for symmetry breaking are summarized in Ref. 6. Most of them are tied to correlating $k_\parallel$ and k_θ via magnetic shear, i.e., $k_\parallel = k_\theta x/L_s$, where $L_s \equiv \hat{s}/Rq$ is the magnetic shear length and x is the

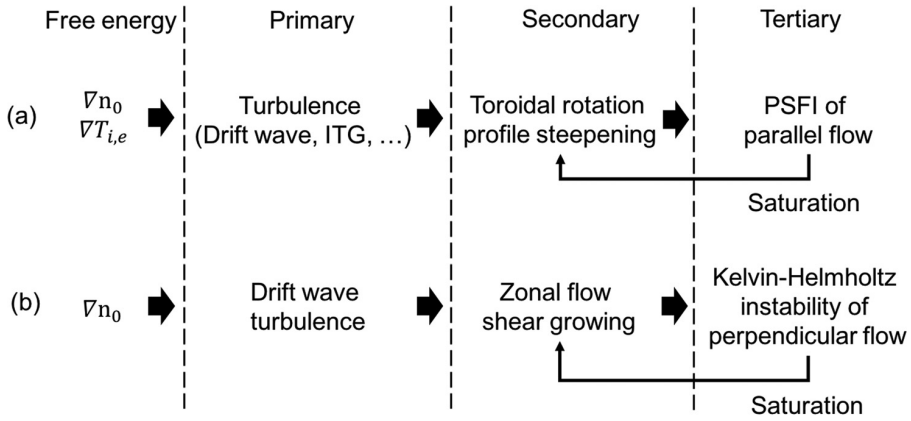

FIG. 1. Primary, secondary, and tertiary effects of free energy sources on (a) intrinsic rotation and (b) zonal flow.

distance between the mode center and the rational surface. Ultimately, the correlator is determined by the spatial distribution of the intensity, i.e., $\langle k_\theta k_\parallel \rangle = k_\theta^2 \langle x \rangle / L_s$.

Conventional symmetry breaking mechanisms, and thus models of intrinsic rotation, require finite magnetic shear. However, residual stress reversal is observed in computer simulations at weak magnetic shear.[17] Moreover, experimental results suggest that a control knob for intrinsic rotation is the magnitude of safety factor q_0 rather than the magnetic shear.[18] Recently, intrinsic parallel flows were observed in a linear device with uniform magnetic field (zero magnetic shear), the Controlled Shear Decorrelation Experiment (CSDX) (Fig. 2).[19] Some of the correspondence between CSDX and tokamaks is summarized in Table I, more of which can be found in Ref. 20. Because neutral gas, as the fuel, is injected radially from the side wall, there is no external source of axial momentum, and so the observed axial flow is intrinsic. In addition, mean axial flow profile steepens during a global transition triggered for a critical axial magnetic field.[20] Meanwhile, the steepening of $\nabla \langle v_z \rangle$ tracks that of ∇n_0.[21] This is consistent with that the intrinsic axial momentum transport is driven by electron drift wave turbulence.

The observed intrinsic axial flows in CSDX raise two questions: (1) what generates the intrinsic axial flow; (2) what determines the mean axial flow profile? Intrinsic toroidal flows are driven by the residual axial stress Π_{rz}^{Res}, which requires spectral symmetry breaking. However, conventional symmetry breaking mechanisms do not apply to CSDX due to the uniform magnetic field there, i.e., zero magnetic shear. Motivated by these observations, in this paper, we propose a new dynamical symmetry breaking mechanism which does not require a specific magnetic field structure. In this model, we consider a drift wave system with weakly nonadiabatic electrons ($\tilde{n}_e/n_0 = (1 - i\delta)\tilde{\phi}$ with $0 < \delta \ll 1$) in the presence of finite axial flow shear. By dynamical symmetry breaking, we mean that a small but finite perturbation to the mean axial flow profile can break the symmetry, and the resulting turbulence spectral imbalance sets a finite residual stress. The residual stress driven intrinsic flow then adds to the initial flow profile perturbation. Therefore, the flow profile perturbation is self-amplified via a closed feedback loop, as in a modulational instability. The residual stress gives rise to a momentum flux with a negative diffusivity, $\Pi_{rz}^{\mathrm{Res}} \sim |\chi_\phi^{\mathrm{Res}}| \langle v_z \rangle'$, inducing a negative increment $(-|\chi_\phi^{\mathrm{Res}}|)$ to the ambient turbulent viscosity (χ_ϕ). Hence, the dynamical symmetry breaking is essentially a negative viscosity phenomenon. The growth of axial flow shear by the dynamical symmetry breaking is analogous to the modulational growth of zonal flow shear.[13]

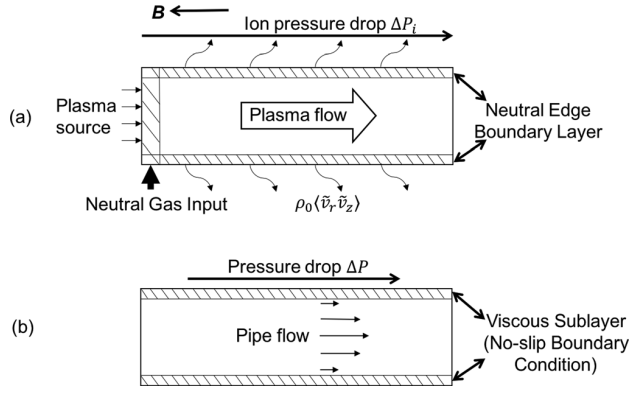

FIG. 2. (a) Sketch of axial plasma flow in CSDX in analogy to (b) turbulent pipe flow.

The mean axial flow can be driven by an axial ion pressure drop and is enhanced by the negative viscosity. As shown in Fig. 2, the helicon source on the left end of the cylinder makes the nearby plasma hotter than the plasma near the endplate, thus giving rise to an axial ion pressure drop, $\Delta P_i = P_i|_{\mathrm{Source}} - P_i|_{\mathrm{Endplate}}$. Hence, in analogy to the turbulent hydrodynamic pipe flows, the axial plasma flow in a linear device is driven by ΔP_i and dissipated by the total viscosity, consisting of both the ambient turbulent viscosity and the negative viscosity increment induced by the residual stress, i.e., $\langle v_z \rangle' \sim \Delta P_i / (\chi_\phi - |\chi_\phi^{\mathrm{Res}}|)$. Therefore, with external excitation (e.g., ΔP_i), a total negative viscosity is *not* needed to generate axial flows, and $\langle v_z \rangle'$ is enhanced by $-|\chi_\phi^{\mathrm{Res}}|$. In addition, boundary conditions must be considered to determine the mean flow profile.[22] In CSDX, the boundary layer is dominated by neutral flows (Fig. 2). The outer region of the cylindrical plasma is only partially ionized, and the neutral momentum is coupled to the plasma momentum via the ionization and recombination processes within the boundary layer. Thus, the neutral dynamics in the boundary layer plays a role in the boundary conditions for the plasma flow in the center.

Driven by electron drift wave turbulence with no requirement for magnetic field geometry, the dynamical symmetry

TABLE I. Correspondence between the linear device, CSDX, and tokamaks.

Tokamaks	CSDX
Most have sheared magnetic field	Uniform axial magnetic field (shear-free)
Intrinsic toroidal rotation	Intrinsic axial flow
Rotation boundary condition set by SOL	Axial flow boundary condition set by boundary neutral layer

breaking is applicable to intrinsic rotation in flat q regions[23,24] where conventional models fail, as well as to intrinsic rotation in plasmas where the electron channel (and thus CTEM) is dominant. Also, a total negative viscosity, as well as the underlying modulational growth of test flow shear, is not needed to generate intrinsic rotation at normal magnetic shears, because the residual stress determined by conventional symmetry breaking mechanisms can accelerate the plasma. Therefore, the profile gradient of intrinsic toroidal rotation is *enhanced* by the negative viscosity induced by the dynamical symmetry breaking, i.e., $\langle v_\parallel \rangle' \sim \Pi_{r\parallel}^{\mathrm{Res}}/(\chi_\phi - |\chi_\phi^{\mathrm{Res}}|)$.

To summarize, the new dynamical symmetry breaking mechanism discussed here is outside the domain of conventional models of residual stress. The contrast and comparison are summarized in Table II. The dynamical symmetry breaking is different in two ways: (1) Intrinsic flow is generated by the self-amplification of a test or seed flow shear. This process is driven fundamentally by ∇n_0, i.e., as in a modulational instability of drift waves, similar to the modulational growth of zonal flow shear. (2) Instead of an intrinsic torque that accelerates the flow, the dynamical symmetry breaking mechanism yields a residual stress which induces a negative increment to the ambient turbulent viscosity that enhances the mean flow profile gradient.

The rest of this paper is organized as follows: Sec. II introduces the derivation of the drift wave system coupled to axial flow fluctuations in the weakly nonadiabatic limit; Sec. III discusses the dynamical symmetry breaking mechanism; Sec. IV elaborates the negative viscosity induced by the residual stress; the total axial flow structure is calculated and discussed in Sec. V; Sec. VI gives the implications for tokamaks of dynamical symmetry breaking; Sec. VII summarizes and discusses the results.

II. PHYSICS MODEL

We consider a system consisting of electron density, electron axial momentum, charge balance, and plasma axial flow in cylindrical geometry where magnetic field is uniform in the axial direction

$$\frac{\mathrm{D}\tilde{n}_e}{\mathrm{D}t} + \mathbf{v}_E \cdot \nabla n_0 + n_0 \frac{\partial \tilde{v}_e}{\partial z} = 0, \tag{2}$$

$$m_e n_0 \frac{\mathrm{D}}{\mathrm{D}t}\tilde{v}_e = e n_0 \frac{\partial \tilde{\phi}}{\partial z} - \frac{\partial \tilde{p}_e}{\partial z} - \nu_{\mathrm{ei}} m_e n_0 \tilde{v}_e, \tag{3}$$

$$\nabla_\perp \cdot \mathbf{j}_\perp = -\frac{\partial j_z}{\partial z}, \tag{4}$$

$$\frac{\mathrm{D}}{\mathrm{D}t}\tilde{v}_z + \mathbf{v}_E \cdot \nabla \langle v_z \rangle = -\frac{\partial \tilde{p}_e}{\partial z}. \tag{5}$$

Here, $\mathrm{D}/\mathrm{D}t \equiv \partial_t + \mathbf{v}_E \cdot \nabla$ is the convective time derivative and $\mathbf{v}_E = \hat{z} \times \nabla\tilde{\phi}$ is the $E \times B$ drift velocity. In the following analysis, it is convenient to normalize the quantities as follows: $\tilde{n} \equiv \tilde{n}_e/n_0$, $\tilde{\phi} \equiv e\tilde{\phi}/T_e$, length $\equiv$ length$/\rho_s$, $t \equiv t/\omega_{ci}$, $\tilde{v}_z \equiv \tilde{v}_z/c_s$, where $c_s \equiv \sqrt{T_e/m_i}$ is the ion acoustic speed, $\omega_{ci} \equiv eB/m_i$ is the ion cyclotron frequency, and $\rho_s \equiv c_s/\omega_{ci}$. The perpendicular current is set by the polarization current $\mathbf{j}_\perp = -n_0 \frac{D}{Dt}\nabla_\perp \tilde{\phi}$, while the axial current is $j_z = n_0(\tilde{v}_z - \tilde{v}_e)$. Thus, the electron flow is cancelled by subtracting Eq. (4) from Eq. (2)

$$\frac{\mathrm{D}}{\mathrm{D}t}\left(\tilde{n} - \nabla_\perp^2 \tilde{\phi}\right) + \frac{1}{L_n}\frac{1}{r}\frac{\partial \tilde{\phi}}{\partial \theta} + \frac{\partial \tilde{v}_z}{\partial z} = 0, \tag{6}$$

where $L_n \equiv -(d \ln n_0/dr)^{-1}$ is the density profile gradient length. Ion pressure fluctuation is neglected in the flow equation, since $\tilde{p}_i \ll \tilde{p}_e$. In the presence of a finite mean axial flow shear $\langle v_z \rangle'$, the axial flow momentum equation becomes

TABLE II. Compare and contrast the dynamical symmetry breaking with conventional symmetry breaking mechanisms.

	Standard symmetry breaking	Dynamical symmetry breaking
Free energy	$\nabla T_i, \nabla n_0, \ldots$	∇n_0
Symmetry breaker	$E_r', I(x)', \ldots$ All tied to magnetic field configuration	Test axial flow shear, $\delta\langle v_z \rangle'$; No requirement for shear of $\boldsymbol{B}$ structure
Effect on flow	Instruction, $\partial_r \prod_{r\parallel}^{Res}$	Negative viscosity, $-\lvert\chi^{Res}\rvert$ driven by ∇n_0
Flow profile	$\langle v_\parallel \rangle' = \frac{\prod_{r\parallel}^{Res}}{\chi_\phi}$	$\langle v_Z \rangle' = \frac{\text{Flow drive}\left(\text{e.g. } \prod_{rz}^{Res}, \Delta P_i\right)}{\chi_\phi(\nabla N_0, \nabla\langle v_z \rangle) - \lvert\chi_\phi^{Res}\rvert}$
Feedback loop	Heat flux → ∇T_i + geometry (magnetic shear); Open loop; $\Pi_{r\parallel}^{Res}$ → $\langle v_\parallel \rangle'$	Test flow shear $\delta\langle v_z \rangle'$ → Spectral imbalance; Self-amplification Driven by ∇n_0; Residual stress Π_{rz}^{Res} → Intrinsic flow, feedback on $\delta\langle v_z \rangle'$

$$\frac{\mathrm{D}}{\mathrm{D}t}\tilde{v}_z - \langle v_z\rangle' \frac{1}{r}\frac{\partial\tilde{\phi}}{\partial\theta} = -\frac{\partial\tilde{n}}{\partial z}, \tag{7}$$

where the thermal fluctuations of electrons are ignored, such that $\tilde{p}_e = T_e\tilde{n}$. To close the system, the electron density fluctuation needs to be evaluated. The electron response is nearly adiabatic, i.e., $\tilde{n} = (1 - i\delta)\tilde{\phi}$ with $\delta \ll 1$, given by Eqs. (2) and (3). The electron axial momentum is damped by electron–ion collisions. With the electrons in the thermal equilibrium state $\nu_{ei} \gg \omega$, the inertia term in Eq. (3) can be neglected. As a consequence, the electron current is driven by the nonadiabatic electrons

$$\tilde{v}_e = -\frac{v_{The}^2}{\nu_{ei}}\frac{\partial}{\partial z}\left(\tilde{n} - \tilde{\phi}\right). \tag{8}$$

In the weakly nonadiabatic limit, $1 < k_z^2 v_{The}^2/(\nu_{ei}\omega_k) < \infty$. Plugging the electron current into the electron density equation, the nonadiabatic electron response is then given by

$$\delta \cong \frac{\nu_{ei}(\omega_* - \omega_k)}{k_z^2 v_{The}^2}, \tag{9}$$

where $\omega_* \equiv k_\theta \rho_s c_s/L_n$ is the electron drift frequency. In the weakly nonadiabatic limit, $0 < \delta \ll 1$. For adiabatic electrons, $k_z^2 v_{The}^2/(\nu_{ei}\omega_k) \to \infty$, then $\delta \to 0$ and $\tilde{n} \to \tilde{\phi}$. Finally, we arrive at the drift wave system with weakly nonadiabatic electrons coupled to the axial flow fluctuations

$$\frac{\mathrm{D}}{\mathrm{D}t}\left(1 - i\delta - \nabla_\perp^2\right)\tilde{\phi} + \frac{1}{L_n}\frac{1}{r}\frac{\partial\tilde{\phi}}{\partial\theta} + \frac{\partial\tilde{v}_z}{\partial z} = 0, \tag{10}$$

$$\frac{\mathrm{D}}{\mathrm{D}t}\tilde{v}_z - \langle v_z\rangle' \frac{1}{r}\frac{\partial\tilde{\phi}}{\partial\theta} = -(1 - i\delta)\frac{\partial\tilde{\phi}}{\partial z}, \tag{11}$$

with δ given by Eq. (9). This system gives two instabilities: electron drift wave instability and parallel shear flow instability (PSFI). The electron drift wave is unstable in the presence of nonadiabatic electrons and is driven by ∇n_0. Next, we will briefly discuss the PSFI in the presence of nearly adiabatic electrons.

PSFI is driven by $\nabla\langle v_z\rangle$ and is essentially a negative compressibility phenomenon. The dispersion relation for the coupled system (Eqs. (10) and (11)) is

$$1 + k_\perp^2\rho_s^2 - i\delta - \frac{\omega_*}{\omega} + \frac{k_\theta k_z \rho_s c_s \langle v_z\rangle'}{\omega^2} - (1 - i\delta)\frac{k_z^2 c_s^2}{\omega^2} = 0, \tag{12}$$

where $0 < \delta \ll 1$ in the weakly nonadiabatic limit. As a quadratic equation of ω, Eq. (12) gives unstable solution when the mean flow shear $\langle v_z\rangle'$ exceeds a critical value

$$\langle v_z\rangle'_{crit} = \frac{1}{k_\theta k_z \rho_s c_s}\left[\frac{\omega_*^2\left(1 + k_\perp^2\rho_s^2\right)}{4\left[\left(1 + k_\perp^2\rho_s^2\right)^2 + \delta^2\right]} + k_z^2 c_s^2\right], \tag{13}$$

such that the discriminant is negative. If the drift wave branch is neglected, the dispersion relation (Eq. (12)) supports a modified ion acoustic wave

$$\omega^2 \sim \gamma^{eff} k_z^2 c_s^2, \tag{14}$$

with the effective compressibility of the axial flow as

$$\gamma^{eff} = \frac{1}{1 + k_\perp^2\rho_s^2}\left(1 - \frac{k_\theta\langle v_z\rangle'}{k_z\omega_{ci}}\right). \tag{15}$$

When the axial flow shear is large enough such that the compressibility becomes negative, the modified ion acoustic wave is driven unstable. Therefore, the PSFI is driven by negative compressibility.

With the coupled drift wave system in the weakly nonadiabatic limit, next, we will show how this system breaks the spectral symmetry of the drift wave turbulence.

III. DYNAMICAL SYMMETRY BREAKING

Consider the axial flows in a linear cylindrical plasma. The dynamics of the mean axial flow is governed by

$$\frac{\partial\langle v_z\rangle}{\partial t} + \frac{\partial\langle\tilde{v}_r\tilde{v}_z\rangle}{\partial r} = -\frac{1}{\rho_0}\frac{\partial P_i}{\partial z} - \nu_{ni}\left(\langle v_z\rangle - \langle v_{z,n}\rangle\right). \tag{16}$$

The mean ion pressure drops in the axial direction due to the axially inhomogeneous ion temperature (Fig. 2) and thus can drive a mean flow $\langle v_z\rangle$, even though its fluctuation was neglected in the fluctuation equation of axial flow. While ΔP_i drives the axial flow in the center region, the boundary layer is controlled by the collisional coupling between plasma flows ($\langle v_z\rangle$) and neutral flows ($\langle v_{z,n}\rangle$). The generic form of the Reynolds stress is given by

$$\langle\tilde{v}_r\tilde{v}_z\rangle = -\chi_\phi\frac{\partial\langle v_z\rangle}{\partial r} + \Pi_{rz}^{Res}. \tag{17}$$

The momentum pinch is ignored because (1) there is no toroidal effect in the linear device, where the magnetic fields lines are straight and uniform, and (2) the pinch effect is responsible for redistribution of the axial momentum but not for generation.

To calculate the Reynolds stress $\langle\tilde{v}_r\tilde{v}_z\rangle$, linearize Eq. (11) to get the linear response for the axial velocity fluctuation $\tilde{v}_z$, and $\tilde{v}_r$ is the fluctuation of the radial $E \times B$ velocity. The quasilinear Reynolds stress is then determined by the cross phase between $\tilde{v}_r$ and $\tilde{v}_z$

$$\langle\tilde{v}_r\tilde{v}_z\rangle = -\sum_k \frac{|\gamma_k|}{\omega_k^2}k_\theta^2\rho_s^2|\phi_k|^2\langle v_z\rangle' + \sum_k\left(\frac{|\gamma_k|}{\omega_k^2} + \frac{\delta}{\omega_k}\right)k_\theta k_z\rho_s c_s|\phi_k|^2, \tag{18}$$

where γ_k and ω_k arise from the drift wave system. The residual stress (the second term in Eq. (18)) is determined by the correlator, i.e., $\Pi_{rz}^{Res} \sim \langle k_\theta k_z\rangle \equiv \sum_k k_\theta k_z|\phi_k|^2$, which requires spectral imbalance, due to correlated $\tilde{v}_r$ and $\tilde{v}_z$ fluctuations.

The coupled system described by Eqs. (10) and (11) is controlled by drift wave modes when $\langle v_z\rangle'$ is below the PSFI threshold. This drift wave dominated system is unstable due to nonadiabatic electrons (which set the cross phase between electron density perturbation and electrostatic potential perturbation). Specifically, the linear growth rate is set by the weakly nonadiabatic electron density perturbation as

$$\gamma_k \cong \omega_* \delta/(1+k_\perp^2\rho_s^2)^2, \tag{19}$$

given by the dispersion relation (Eq. (12)) with the ion-acoustic branch neglected. With δ given by Eq. (9), the linear growth rate of the collisional drift wave is then set by the frequency shift from the electron drift frequency

$$\gamma_k \cong \frac{\nu_{ei}}{k_z^2 v_{The}^2}\frac{\omega_*(\omega_* - \omega_k)}{\left(1+k_\perp^2\rho_s^2\right)^2}. \tag{20}$$

The frequency of the system is controlled by the electron drift frequency with a shift set by the mean axial flow shear

$$\omega_k \cong \frac{\omega_*}{1+k_\perp^2\rho_s^2} - \frac{k_\theta k_z \rho_s c_s \langle v_z\rangle'}{\omega_*}. \tag{21}$$

Consequently, the full expression for the growth rate is

$$\gamma_k \cong \frac{\nu_{ei}}{k_z^2 v_{The}^2}\frac{\omega_*^2}{\left(1+k_\perp^2\rho_s^2\right)^2}\left(\frac{k_\perp^2\rho_s^2}{1+k_\perp^2\rho_s^2} + \frac{k_\theta k_z \rho_s c_s \langle v_z\rangle'}{\omega_*^2}\right). \tag{22}$$

With ∇n_0 as the free energy source, a finite mean axial flow shear can break the symmetry of the background drift wave turbulence. For a flat mean axial flow profile, i.e., $\langle v_z\rangle' = 0$, the growth rate given by Eq. (22) is symmetric for $k_z \to -k_z$. The resulting turbulence spectrum is consequently expected to be symmetric in **k** space, giving $\Pi_{rz}^{Res} \sim \langle k_\theta k_z\rangle = 0$. The momentum diffusion is also zero for the flat mean flow profile. Therefore, the mean axial flow profile is stationary and stays flat. However, a small but finite perturbation to the mean flow profile, e.g., $\delta\langle v_z\rangle' > 0$, breaks the symmetry of the background turbulence. With larger linear growth rates, modes with $k_\theta k_z > 0$, whose frequencies shift further away from ω_*, grow faster than the other modes. The drift wave turbulence intensity is then unbalanced in $k_\theta k_z$ space (Fig. 3). Hence, k_θ and k_z are correlated by the spectral imbalance, and so form a finite residual stress, since $\Pi_{rz}^{Res} \sim \langle k_\theta k_z\rangle > 0$. This residual stress amplifies the initial test flow shear, closing the feedback loop for the self-amplification of test flow shear (Table II).

Given the drift wave instability in the background and the spectral imbalance resulting from the symmetry breaking, the Reynolds stress can be calculated. The first term in the Reynolds stress Eq. (18) is a diffusive axial momentum flux, with the turbulent viscosity

$$\chi_\phi \cong \sum_k \frac{\nu_{ei}}{k_z^2 v_{The}^2}\frac{k_\perp^2\rho_s^2}{1+k_\perp^2\rho_s^2} k_\theta^2\rho_s^2|\phi_k|^2. \tag{23}$$

This turbulent viscosity is driven by the ambient background turbulence. So, for the drift wave turbulence dominated case, χ_ϕ is driven primarily by ∇n_0. Additionally, as will be discussed later, the PSFI will enter when $\langle v_z\rangle' > \langle v_z\rangle'_{crit}$. Then, the turbulent viscosity is driven by both density gradient and the mean flow gradient, i.e., $\chi_\phi = \chi_\phi^{DW}(\nabla n_0) + \chi_\phi^{PSFI}(\nabla\langle v_z\rangle)\Theta(\langle v_z\rangle' - \langle v_z\rangle'_{crit})$, where $\Theta(x)$ is a Heaviside step function, acting as a switch for the onset of PSFI driven turbulence.

The off-diagonal flux in Eq. (18) is the residual stress

$$\Pi_{rz}^{Res} \cong \sum_k \frac{\nu_{ei}}{k_z^2 v_{The}^2}\left(2+k_\perp^2\rho_s^2\right) \times \left[\underbrace{\frac{k_\perp^2\rho_s^2}{1+k_\perp^2\rho_s^2}}_{①} + \underbrace{\frac{k_\theta k_z \rho_s c_s\langle v_z\rangle'}{\omega_*^2}}_{②}\right] k_\theta k_z \rho_s c_s |\phi_k|^2. \tag{24}$$

Π_{rz}^{Res} is dominated by term ① when $\langle v_z\rangle'$ is below the PSFI threshold. Hence, in the presence of a finite test axial flow shear, the spectral imbalance in Fig. 3 gives rise to the residual stress

$$\Pi_{rz}^{Res} = \mathrm{sgn}\left(\delta\langle v_z\rangle'\right)\sum_{\{k+\}}\frac{\nu_{ei}}{k_z^2 v_{The}^2}\left(2+k_\perp^2\rho_s^2\right) \times \frac{k_\perp^2\rho_s^2}{1+k_\perp^2\rho_s^2}|k_\theta k_z|\rho_s c_s \Delta I_k\left(\delta\langle v_z\rangle'\right), \tag{25}$$

where $\Delta I_k(\delta\langle v_z\rangle') = |\phi_k|^2|_{\{k+\}} - |\phi_k|^2|_{\{k-\}}$ accounts for the spectral imbalance. On account of the symmetry breaking term in the growth rate Eq. (22), the residual stress has the same sign as $\delta\langle v_z\rangle'$. Moreover, Π_{rz}^{Res} depends explicitly on the mean axial flow shear via term ② in Eq. (24) as well as via the spectral imbalance. Term ② $\sim \sum_k k_\theta^2/\omega_*^2|\phi_k|^2\delta\langle v_z\rangle' = L_n^2\sum_k|\phi_k|^2\delta\langle v_z\rangle'$ does not require symmetry breaking and enters in the form of a negative diffusion. Therefore, a negative viscosity increment is induced by the residual stress.

It should be noted that the dependence of residual stress upon $\delta\langle v_z\rangle'$ cannot be absorbed by the diffusive component of the Reynolds stress for 3 reasons: (1) the magnitude of residual stress is dominated by term ① of Eq. (24) which is independent of $\delta\langle v_z\rangle'$; (2) the spectral imbalance is induced via

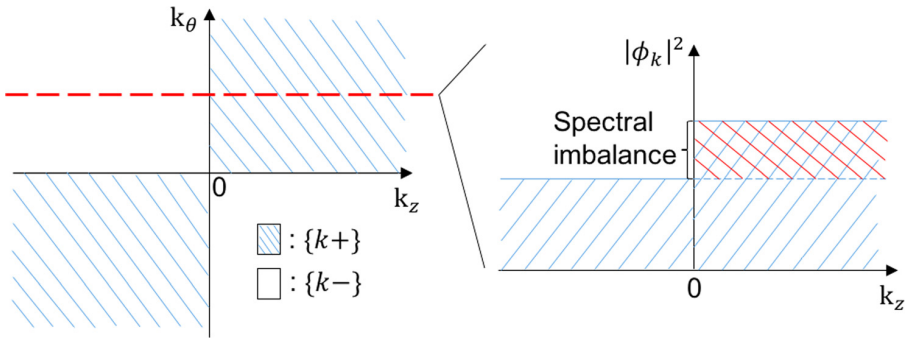

FIG. 3. Spectral imbalance in $k_\theta k_z$ space.

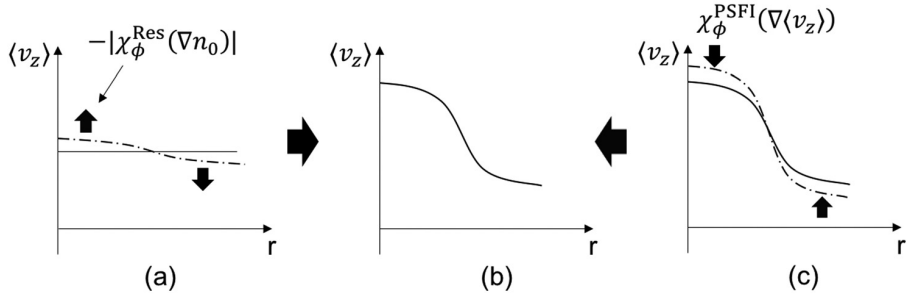

FIG. 4. Modulational growth of the test flow shear. (a) Perturbation to the axial flow profile is self-amplified by the modulational instability driven by residual stress induced negative viscosity $-|\chi_\phi^{\rm Res}(\nabla n_0)|$. (b) The test flow shear is amplified into a macroscopic profile. (c) When the axial flow shear hits the PSFI threshold, the additional $\chi_\phi^{\rm PSFI}(\nabla\langle v_z\rangle)$ relaxes the flow profile, keeping $\langle v_z\rangle'$ at or below $\langle v_z\rangle'_{\rm crit}$.

both linear growth and nonlinear saturation of modes, so $\Delta I_k(\delta\langle v_z\rangle')$ and thus $\Pi_{rz}^{\rm Res}$ are essentially nonlinear in $\delta\langle v_z\rangle'$; (3) even the term linear in $\delta\langle v_z\rangle'$ results in a negative diffusive flux rather than a positive, downgradient diffusion. The induced negative viscosity can give rise to the modulational growth of the test flow shear, as will be shown in Section IV.

IV. NEGATIVE VISCOSITY

The dynamical symmetry breaking mechanism is essentially the self-amplification of test flow shear, driven by drift wave turbulence, which is similar to the modulational growth of zonal flow shear. In this section, the growth and saturation of the test flow shear are considered. The modulational growth of the test flow shear is illustrated by the cartoon in Fig. 4. The dynamics of the test flow shear is a diffusion process with the turbulent viscosity as the effective diffusivity. We will show that the residual stress induces a negative increment to the ambient turbulent viscosity. Thus, the total viscosity is $\chi_\phi^{\rm tot}=\chi_\phi-|\chi_\phi^{\rm Res}|$. When $|\chi_\phi^{\rm Res}|$ is strong enough such that the total viscosity becomes negative, the test flow shear will grow until the flow shear hits the PSFI threshold given by Eq. (13). Then, the additional turbulent viscosity induced by PSFI turbulence makes the total viscosity positive and stops the growth of the test flow shear $\langle v_z\rangle'_{\rm crit}$, thus sets an effective upper limit for the profile gradient of axial flow.

The dynamics of the test flow shear can be derived from Eq. (16)

$$\frac{\partial\delta\langle v_z\rangle'}{\partial t}+\frac{\partial^2}{\partial r^2}\left(-\chi_\phi\delta\langle v_z\rangle'+\delta\Pi_{rz}^{\rm Res}\right)=0. \tag{26}$$

Without the perturbed residual stress, the dynamics of the test flow shear is a diffusion process with the flow shear flux $\Gamma_{\delta\langle v_z\rangle'}=-\chi_\phi\partial_r\delta\langle v_z\rangle'$. Next, we will show that the residual stress due to the perturbed axial flow shear induces a momentum flux with a negative diffusivity. The test flow shear flux is then modified by the negative increment of momentum diffusivity.

To do this, we begin by calculating the perturbed residual stress. Given by Eq. (18), the residual stress explicitly depends on the flow shear through the growth rate and the frequency. Moreover, the turbulence intensity depends on the flow shear because of the spectral imbalance induced by $\langle v_z\rangle'$. Therefore, it is convenient to write the turbulence intensity in terms of the wave action density, which is, by definition, $N_k\equiv\varepsilon_k/\omega_k$. Here, the wave energy of the electron drift wave is $\varepsilon_k=\frac{1}{2}(1+k_\perp^2\rho_s^2)^2|\phi_k|^2$.[25] Consequently, the perturbed residual stress due to the test flow shear can be written as $\delta\Pi_{rz}^{\rm Res}=\delta\Pi_{rz}^{\rm Res}(\delta\gamma_k,\delta\omega_k,\delta N_k)$. The perturbed growth rate and perturbed frequency are calculated directly from Eqs. (21) and (22), while the perturbed wave action density due to the axial flow profile perturbation is calculated as follows.

The wave action density $N_k\equiv\varepsilon_k/\omega_k$ is essentially the population of waves with wave number $\mathbf{k}$. Its dynamics is governed by the wave kinetic equation

$$\frac{\partial N_k}{\partial t}+v_{gr}\frac{\partial N_k}{\partial r}-\frac{\partial}{\partial r}(\omega_k+\mathbf{k}\cdot\mathbf{V})\frac{\partial N_k}{\partial k_r}=\gamma_k N_k-\Delta\omega_k\frac{N_k^2}{N_0}. \tag{27}$$

We separate the perturbation, due to test flow shear, from the slowly varying mean wave action density, i.e., $N_k=\delta N_k+\langle N_k\rangle$. The linearized equation for δN_k is then

$$\frac{\partial\delta N_k}{\partial t}+\delta v_{gr}\frac{\partial\langle N_k\rangle}{\partial r}-\frac{\partial}{\partial r}\delta(\omega_k+\mathbf{k}\cdot\mathbf{V})\frac{\partial\langle N_k\rangle}{\partial k_r}=\gamma_k\delta N_k+\delta\gamma_k\langle N_k\rangle-2\Delta\omega_k\delta N_k. \tag{28}$$

The convection by the wave packet motion vanishes because

$$\frac{\delta v_{gr}}{\delta\langle v_z\rangle'}=\frac{\delta(\partial\omega_k/\partial k_r)}{\delta\langle v_z\rangle'}=0,$$

where only the linear frequency shift is considered. Ignoring the zonal flow effects, since there is no coupling between k_θ and k_z by geometry, the refraction term becomes

$$\frac{\partial}{\partial r}\delta(\omega_k+\mathbf{k}\cdot\mathbf{V})\frac{\partial N_k}{\partial k_r}=\left(\frac{\partial\delta\omega_k}{\partial r}+k_z\delta\langle v_z\rangle'\right)\frac{\partial\langle N_k\rangle}{\partial k_r}. \tag{29}$$

The shearing of the frequency perturbation is calculated from Eq. (21)

$$\frac{\partial\delta\omega_k}{\partial r}=k_z\delta\langle v_z\rangle'\left(\frac{L_n^2}{n_0}\frac{\partial^2 n_0}{\partial r^2}-1\right). \tag{30}$$

Thus, the perturbation to the refraction term is driven by the density profile curvature

$$\delta\left\{\frac{\partial}{\partial r}(\omega_k+\mathbf{k}\cdot\mathbf{V})\frac{\partial N_k}{\partial k_r}\right\}=k_z\delta\langle v_z\rangle'\frac{L_n^2}{n_0}\frac{\partial^2 n_0}{\partial r^2}\frac{\partial\langle N_k\rangle}{\partial k_r}. \tag{31}$$

Here, we consider the drift wave turbulence with finite ∇n_0, so the effect of $\partial n_0/\partial r$ is dominant over that of $\partial^2 n_0/\partial r^2$, and thus, the above curvature driven term (Eq. (31)) can be neglected. Therefore, δN_k is driven by the linear growth and nonlinear self-interaction of drift waves

$$\frac{\partial \delta N_k}{\partial t} = \gamma_k \delta N_k + \delta\gamma_k \langle N_k \rangle - 2\Delta\omega_k \delta N_k. \tag{32}$$

The steady state perturbation is then given by

$$\delta N_k = \frac{\delta\gamma_k}{2\Delta\omega_k - \gamma_k} \langle N_k \rangle, \tag{33}$$

where the decorrelation rate $\Delta\omega_k \cong \gamma_k$ is determined by the steady state equilibrium, $\langle N_k \rangle$. Finally, with the perturbed growth rate calculated from Eq. (22), the perturbed wave action density due to the test flow shear is

$$\delta N_k = \frac{1 + k_\perp^2 \rho_s^2}{k_\perp^2 \rho_s^2} \frac{k_\theta k_z \rho_s c_s \delta \langle v_z \rangle'}{\omega_*^2} \langle N_k \rangle. \tag{34}$$

Thus, the perturbed residual stress due to the test flow shear takes the form of a negative diffusive flux of axial momentum

$$\delta \Pi_{rz}^{\mathrm{Res}} \equiv -\chi_\phi^{\mathrm{Res}} \delta \langle v_z \rangle', \tag{35}$$

with the negative viscosity

$$\chi_\phi^{\mathrm{Res}} = -\frac{\nu_{\mathrm{ei}} L_n^2}{v_{\mathrm{The}}^2} \sum_k \left(1 + k_\perp^2 \rho_s^2\right)\left(4 + k_\perp^2 \rho_s^2\right) |\phi_k|^2, \tag{36}$$

related to Π_{rz}^{Res} by dynamical symmetry breaking. Therefore, the test flow shear dynamics is a diffusion process

$$\frac{\partial \delta \langle v_z \rangle'}{\partial t} - \frac{\partial^2}{\partial r^2} \chi_\phi^{\mathrm{tot}} \delta \langle v_z \rangle' = 0, \tag{37}$$

where the total viscosity

$$\chi_\phi^{\mathrm{tot}} = \chi_\phi - |\chi_\phi^{\mathrm{Res}}|, \tag{38}$$

consists of both the ambient turbulent viscosity and the negative viscosity induced by the residual stress. Thus, an axial flow shear modulation is either damped or growing without oscillation, with growth rate given by

$$\gamma_q = -q_r^2 \chi_\phi^{\mathrm{tot}}, \tag{39}$$

where q_r is the radial wave number of the modulation. When the negative viscosity is large enough that the total viscosity becomes negative, the axial flow shear modulation is unstable, which means a small perturbation to the mean flow profile can be amplified. This is analogous to the modulational growth of zonal flow shears.[13]

However, the test flow shear cannot grow forever. The mean axial flow profile gradient is limited by the PSFI threshold Eq. (13). When the flow shear hits $\langle v_z \rangle'_{\mathrm{crit}}$, an additional turbulent viscosity $\chi_\phi^{\mathrm{PSFI}}$ driven by $\nabla\langle v_z \rangle$ is induced. Moreover, being nonlinear in the flow shear, $\chi_\phi^{\mathrm{PSFI}}$ is large enough to make the total viscosity positive, since

$$\chi_\phi^{\mathrm{tot}} = \chi_\phi^{\mathrm{DW}} + \chi_\phi^{\mathrm{PSFI}} \Theta(\langle v_z \rangle' - \langle v_z \rangle'_{\mathrm{crit}}) - |\chi_\phi^{\mathrm{Res}}|, \tag{40}$$

so that the modulational growth of the test flow shear stops. In this way, the PSFI threshold given by Eq. (13) sets an upper limit for the mean flow shear driven by the modulational growth, and the total viscosity is kept positive.

To summarize, a test, or seed, sheared axial flow is amplified by the negative viscosity induced by the residual stress. In particular, when the induced negative viscosity is larger than the ambient turbulent viscosity such that the total viscosity becomes negative, the test shear is then amplified to form a macroscopic profile by the modulational instability. The axial flow profile gradient is limited by the PSFI threshold. Also, the total viscosity stays positive due to the PSFI induced turbulent viscosity. Moreover, the total viscosity given by Eq. (40) is driven by both ∇n_0 (which drives χ_ϕ^{DW} and $-|\chi_\phi^{\mathrm{Res}}|$) and $\nabla\langle v_z \rangle$ (which drives $\chi_\phi^{\mathrm{PSFI}}$ when PSFI switches on). This makes χ_ϕ^{tot} different from familiar eddy viscosities. In particular, χ_ϕ^{tot} can give rise to the self-amplification of a test flow shear and also limit this modulational growth.

V. MEAN FLOW STRUCTURE

The turbulent plasma flow in a cylindrical chamber is similar to a turbulent pipe flow (Fig. 2), with a point-by-point comparison listed in Table III. The turbulent hydrodynamic pipe flow is driven by axial pressure drop due to pumping power, and dissipated by the turbulent viscosity driven by the background hydrodynamic turbulence. By balancing the local momentum input (ΔP) and momentum diffusion ($\langle \tilde{v}_r \tilde{v}_z \rangle \sim -\nu_T \langle v_z \rangle'$), the flow gradient is obtained as $\langle v_z \rangle' \sim -\Delta P/\nu_T$. The flow vanishes at the boundary due to the frictional force by the wall, which sets the boundary condition as no-slip. In a linear plasma device like CSDX, axial plasma flow can always be driven by the axial pressure drop ΔP_i. Therefore, the axial flow does not need a negative viscosity for generation. However, by the dynamical symmetry breaking, the axial flow gradient can be enhanced by the negative viscosity increment induced by the residual stress. Hence, an intrinsic axial flow is generated, enhancing the axial flow driven by ΔP_i. Also, for plasma flow, the total viscosity depends on both ∇n_0 and $\nabla\langle v_z \rangle$.

The boundary condition of the plasma flow is controlled by the neutral layer at the edge where the gas is partially ionized, which thus heavily involves the neutral flow dynamics. Meanwhile, the neutral momentum is coupled to the plasma momentum through ionization and recombination processes, so the boundary condition for the plasma flow is ultimately set by the neutral flows in the boundary layer. In this section, boundary conditions and their effects on the flow profile are discussed.

The axial flow profile is given by the ion momentum balance for the turbulent plasma axial flow, as shown in Fig. 2. The ion pressure drop in the axial direction due to heating at the source end is balanced by the momentum out flux through the side wall, as determined by the Reynolds stress

$$\pi R^2 \Delta P_{\mathrm{i}} = \rho_0 \langle \tilde{v}_z \tilde{v}_r \rangle 2\pi R L.$$

Here, R and L are the radius and the length of the cylindrical plasma tube, respectively, and ρ_0 is the mean plasma density. The Reynolds stress consists of both the diffusive axial momentum flux driven by the ambient turbulent viscosity and

TABLE III. Comparison and contrast between hydrodynamic pipe flow and plasma flow in a cylinder.

	Pipe flow	Plasma flow
Drive	Pressure drop ΔP	Ion pressure drop ΔP_i
Boundary condition	No slip wall	Set by neutral flows within boundary layer, located near the wall
Viscosity	ν_T	$\chi_\phi^{\mathrm{DW}}(\nabla n_0)+\chi_\phi^{\mathrm{PSFI}}(\nabla\langle v_z\rangle)\Theta(\langle v_z\rangle'-\langle v_z\rangle'_{\mathrm{crit}})-\lvert\chi_\phi^{\mathrm{Res}}(\nabla n_0)\rvert$

the residual component that induces a negative viscosity increment by the dynamical symmetry breaking

$$\langle\tilde{v}_z\tilde{v}_r\rangle \cong -[\chi_\phi^{\mathrm{DW}}+\chi_\phi^{\mathrm{PSFI}}\Theta(\langle v_z\rangle'-\langle v_z\rangle'_{\mathrm{crit}})-|\chi_\phi^{\mathrm{Res}}|]\langle v_z\rangle'.$$

As a consequence, the mean axial flow profile is

$$\langle v_z\rangle' \cong -\frac{R\Delta P_{\mathrm{i}}}{2\rho_0 L\left[\chi_\phi^{\mathrm{DW}}+\chi_\phi^{\mathrm{PSFI}}\Theta\left(\langle v_z\rangle'-\langle v_z\rangle'_{\mathrm{crit}}\right)-|\chi_\phi^{\mathrm{Res}}|\right]}. \tag{41}$$

The total viscosity that balances the pressure drop sets an upper limit for the flow shear through its dependence upon the mean flow profile, via the PSFI effect. When the axial flow profile steepens such that the axial flow shear exceeds $\langle v_z\rangle'_{\mathrm{crit}}$ (given by Eq. (13)) and the PSFI switches on, the resulting turbulent viscosity $\chi_\phi^{\mathrm{PSFI}}$ adds to the existing viscosity as a positive increment. The enhanced dissipation level then relaxes the flow profile, so that the mean axial flow profile gradient stays *below or at* the PSFI threshold.

Boundary conditions are important to determine the axial flow profile. By integrating Eq. (16), the net axial flow evolution is

$$\frac{\partial}{\partial t}\int_0^R dr\langle v_z\rangle = \int_0^R dr\frac{\Delta P_i}{\rho_0 L}-\langle\tilde{v}_r\tilde{v}_z\rangle|_R. \tag{42}$$

The momentum flux at the center $r=0$ is neglected because both components of the Reynolds stress are driven by the profile gradients, which vanish at the center. Momentum transfer between ions and neutrals cancels and makes no contribution to the net flow. Eq. (42) shows the radial flux of axial momentum at the boundary is a sink of the net axial flow, and the axial pressure drop in the center region is a source. If there is no momentum source/sink, the flow profile should be reversed because the net momentum is conserved (Fig. 5). However, it is not clear if flow reversal occurs in CSDX,[19] and the net axial flow is always positive.[20] This is due to the small momentum flux (because of the no-slip wall condition) at the boundary and the existence of axial ion pressure drop. Axial flow is small at the boundary due to the frictional force by the wall, so $\tilde{v}_z|_R \cong 0$ and thus $\langle\tilde{v}_r\tilde{v}_z\rangle|_R \cong 0$. As a consequence, ΔP_i driven axial flow in the central region (outer region is dominated by neutral flows) raises the net flow magnitude. To calculate the axial flow profile, integrate Eq. (41) to get

$$\langle v_z(r)\rangle = \langle v_z(R)\rangle + \int_r^R dr\frac{R\Delta P_i}{2\rho_0 L\chi_\phi^{\mathrm{tot}}}. \tag{43}$$

The plasma momentum is coupled to the neutral momentum within the boundary layer. There is no momentum loss during ionization and recombination processes, since the plasma source mostly heats electrons. Therefore, within the boundary layer near the wall ($r_b < r < R$)

$$\langle v_z\rangle \cong \langle v_{n,z}\rangle. \tag{44}$$

For the neutral flows within the boundary layer, the outer boundary is set by the frictional wall condition, as in a no-slip boundary condition. Assuming the width of the boundary layer is small compare to L_n, the plasma flow is approximately no-slip at the boundary, i.e.

$$\langle v_z(R)\rangle \cong 0. \tag{45}$$

With the no-slip boundary condition, the axial flow profile is

$$\langle v_z(r)\rangle = \int_r^R dr\frac{R\Delta P_i}{2\rho_0 L\chi_\phi^{\mathrm{tot}}}, \tag{46}$$

which gives rise to a positive net flow driven by the ion pressure drop in axial direction. However, if the boundary condition is not strictly no-slip—i.e., with positive momentum outflux at the boundary (e.g., momentum loss due to ion-neutral coupling within the boundary layer)—then the flow profile can reverse near the wall region. Therefore, to obtain a

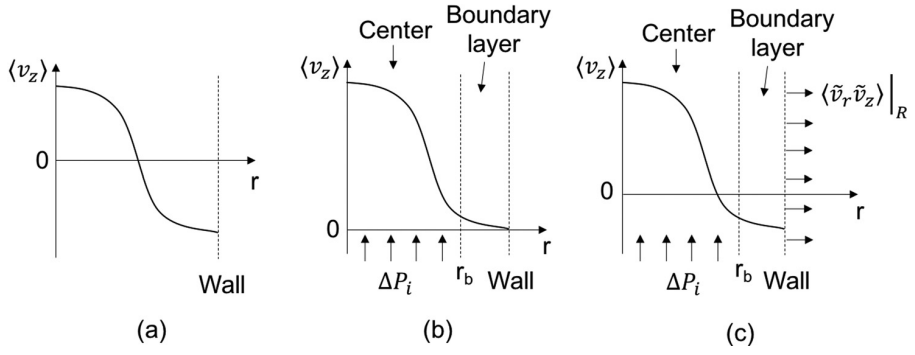

FIG. 5. Mean flow profile for different boundary conditions. (a) No external source/sink. (b) No slip at wall, i.e., momentum flux is zero at the boundary; axial flow is driven by ion pressure drop in the axial direction. (c) With some momentum flux at the wall while axial ion pressure drop dominated, flow profile is reversed with positive net flow.

physical boundary condition for the plasma flow, the details of the coupled ion and neutral dynamics need to be considered within the boundary layer. This is left to future work.

VI. IMPLICATION FOR TOKAMAKS

The dynamical symmetry breaking mechanism does not require a particular magnetic field structure, so it may help understand intrinsic rotations with flat q profile or weak magnetic shear. Recent computational studies discover an intrinsic torque reversal at weak magnetic shear.[17] Moreover, experimental results suggest that the control knob for intrinsic rotation is the magnitude of q_0, rather than magnetic shear.[18] Both of them can be addressed using the dynamical symmetry breaking scheme which is independent from magnetic shear.

We propose a synergy of the conventional residual stress (linked to magnetic shear) and the residual stress induced negative viscosity by dynamical symmetry breaking. For tokamaks with normal magnetic shears, the total viscosity does not need to become negative to generate intrinsic flow, because the intrinsic rotation can be generated by residual stress determined by conventional models. However, the flow dissipation consists of both the ambient turbulent viscosity and the negative viscosity induced by the dynamical symmetry breaking. Then, the mean rotation profile is given by

$$\frac{d\langle v_\parallel\rangle}{dr} = \frac{\Pi_{r\parallel}^{\mathrm{Res}}}{\chi_\phi^{\mathrm{Turb}} - |\chi_\phi^{\mathrm{Res}}|}. \tag{47}$$

Thus, the negative viscosity increment enhances the rotation profile independent of the magnetic field structure. Also, the rotation profile gradient is limited by the PSFI threshold. When $\langle v_\parallel\rangle'$ hits the PSFI threshold, the additional turbulent viscosity driven by PSFI can raise the total viscosity and thus relaxes the rotation profile, since

$$\frac{d\langle v_\parallel\rangle}{dr} = \frac{\Pi_{r\parallel}^{\mathrm{Res}}}{\chi_\phi^{\mathrm{Turb}} + \chi_\phi^{\mathrm{PSFI}}\Theta\left(\langle v_\parallel\rangle' - \langle v_\parallel\rangle'_{\mathrm{PSFI}}\right) - |\chi_\phi^{\mathrm{Res}}|}. \tag{48}$$

As a result, the rotation profile gradient can be expected to stay at or below the PSFI threshold. Therefore, the dynamical symmetry breaking mechanism is applicable to the intrinsic rotation at weak magnetic shear. In addition, as the dynamical symmetry breaking uses a simple model of electron drift wave turbulence, this mechanism can be used to understand the intrinsic rotation in burning plasmas where the turbulence is the CTEM turbulence,[26,27] and to address the effect of electron cyclotron resonance heating (ECRH) on toroidal rotation.[28,29]

VII. CONCLUSION AND DISCUSSION

In this paper, we propose a new dynamical symmetry breaking mechanism for the generation of intrinsic axial flows in linear devices with uniform magnetic field. Specifically, in a simple drift wave system in the presence of finite axial flow shears, a test, or seed, flow shear can be self-amplifying. The linear growth rate of the drift wave instability is set by the frequency shift from the electron drift frequency. A test axial flow shear breaks the symmetry by shifting the frequencies of some classes of modes further away from ω_* than others. As a consequence, the unbalanced turbulence spectrum couples k_θ and k_z, giving rise to a finite residual stress $\Pi_{rz}^{\mathrm{Res}} \sim \langle k_\theta k_z\rangle$. This residual stress amplifies the initial test flow shear by inducing a negative increment to the ambient turbulent viscosity. Thus, this mechanism is essentially one of the negative viscosity. When the negative viscosity induced by residual stress is large enough such that the total viscosity becomes negative, the flow shear modulation is unstable and is amplified by modulational instability. When the axial flow shear exceeds $\langle v_z\rangle'_{\mathrm{crit}}$ and triggers PSFI, the additional turbulent viscosity by PSFI nonlinearly saturates the $\langle v_z\rangle'$ growth. The flow profile will then be relaxed by $\chi_\phi^{\mathrm{PSFI}}$. Hence, the axial flow shear will stay at or below $\langle v_z\rangle'_{\mathrm{crit}}$. Also, the total viscosity given by this model is driven by not only ∇n_0 but also $\nabla\langle v_z\rangle$ due to the PSFI contribution, distinguishing from the standard models of eddy viscosity.

The growth of the test flow shear is analogous to the modulational growth of zonal flow shear. Additionally, the nonlinear saturation by PSFI—a tertiary instability—is similar to the zonal flow saturation by tertiary instability. However, despite these similarities, parallel flow cannot trivially couple to zonal flow via geometry in the linear device, due to the absence of magnetic shear. The simple coupled drift wave system studied here can convert parallel compression $\nabla_\parallel \tilde{v}_\parallel$ into zonal flow,[25] indicating coupling between parallel flow and zonal flow by drift wave turbulence. Thus, zonal flow may play a role in the intrinsic axial flow and the intrinsic toroidal rotation via the parallel flow-zonal flow coupling. This is left to future work.

The self-amplification of test flow shear is energy conserving. Though there is a pressure drop in the axial direction, its direct effect is weak and is amplified by dynamical symmetry breaking. Thus, the axial flow is mainly driven by the background drift wave turbulence. The process of energy transferring between fluctuation and mean axial flow can be illustrated by multiplying the flow fluctuation, mean flow, density fluctuation, mean density, and vorticity equations by $\tilde{v}_z$, $\langle v_z\rangle$, $\tilde{n}_e$, $\langle n\rangle$, ϕ, respectively, and integrating them over the space

$$\frac{\partial}{\partial t}\int \frac{\tilde{v}_z^2}{2} dV = -\int \langle \tilde{v}_r \tilde{v}_z\rangle \frac{\partial \langle v_z\rangle}{\partial r} dV - \int \tilde{v}_z \frac{\partial \tilde{p}_e}{\partial z} dV, \tag{49}$$

$$\frac{\partial}{\partial t}\int \frac{\langle v_z\rangle^2}{2} dV = \int \langle \tilde{v}_r \tilde{v}_z\rangle \frac{\partial \langle v_z\rangle}{\partial r} dV, \tag{50}$$

$$\frac{\partial}{\partial t}\int \frac{\tilde{n}_e^2}{2} dV = -\int \langle \tilde{n}_e \tilde{v}_r\rangle \frac{\partial \langle n\rangle}{\partial r} dV - \int \tilde{n}_e \frac{\partial \tilde{v}_{e,z}}{\partial z} dV, \tag{51}$$

$$\frac{\partial}{\partial t}\int \frac{\langle n\rangle^2}{2} dV = \int \langle \tilde{n}_e \tilde{v}_r\rangle \frac{\partial \langle n\rangle}{\partial r} dV, \tag{52}$$

$$\frac{\partial}{\partial t}\int \frac{(\nabla_\perp \phi)^2}{2} dV = -\int \phi \frac{\partial (\tilde{v}_z - \tilde{v}_{e,z})}{\partial z} dV, \tag{53}$$

where the flow drive by ion pressure drop is neglected since it is weak. By adding them up, we can obtain the energy conservation in the weakly non-adiabatic limit (i.e., $\tilde{n}_e \sim \phi$)

$$\frac{\partial}{\partial t}\int \frac{\tilde{n}_e^2 + (\nabla_\perp \phi)^2 + \tilde{v}_z^2 + \langle v_z\rangle^2 + \langle n\rangle^2}{2} = 0, \qquad (54)$$

where $\tilde{p}_e \cong T_e \tilde{n}_e$ has been used. By keeping track of the couplings between fluctuations and mean profiles in the above system, we can see that energy is coupled in the following progression: $\langle n\rangle \to \tilde{n}_e \to \nabla_\perp \phi$, which is $\tilde{\mathbf{v}}_{E\times B} \to \tilde{v}_z \to \langle v_z\rangle$. Specifically, energy is coupled from $\tilde{v}_z$ to $\langle v_z\rangle$ via the axial Reynolds power $P_z^{\mathrm{Res}} \equiv \langle \tilde{v}_r \tilde{v}_z\rangle \partial_r \langle v_z\rangle$. Thus, it is clear that Reynolds work coupling conserves energy.

In linear device, the axial flow is driven by ion pressure drop in the axial direction and is damped by the total viscosity $\chi_\phi^{\mathrm{tot}} = \chi_\phi^{\mathrm{DW}} + \chi_\phi^{\mathrm{PSFI}}\Theta(\langle v_z\rangle' - \langle v_z\rangle'_{\mathrm{crit}}) - |\chi_\phi^{\mathrm{Res}}|$. The flow profile gradient stays below the PSFI threshold due to the nonlinear saturation by $\chi_\phi^{\mathrm{PSFI}}$. The net axial flow has a source driven by the axial ion pressure drop in the central region and a sink set by the momentum out flux at the wall. Boundary conditions for the plasma flows are determined by neutral flow dynamics within the boundary layer via ion-neutral coupling. In this paper, flow profiles (a) with no drive by ion pressure drop or momentum flux at the wall, (b) with ion pressure drop and no-slip wall boundary condition, and (c) with both ion pressure drop and momentum loss at the boundary are calculated and discussed, respectively. Flow profiles strongly depend on the boundary condition. Future work on the neutral dynamics within the boundary layer will provide a physical boundary condition for the plasma flow, and will thus lead to a better understanding on the global momentum budget and axial flow structure in linear devices.

For tokamaks, a synergy of conventional models for residual stress and the negative viscosity by dynamical symmetry breaking is proposed. The dynamical symmetry breaking does not require complex magnetic field structure, so it is also applicable to intrinsic rotations in tokamaks. The negative viscosity reduces the total flow damping and thus enhances the intrinsic rotation profile gradient. In particular, the dynamical symmetry breaking works in flat q regimes, so it is significant for controlling transport through the q profile. Also, using only a simple model of electron drift waves, this new model for residual stress can be applied to intrinsic rotation in burning plasmas with CTEM turbulence. Moreover, the dynamical symmetry breaking mechanism is also relevant to intrinsic rotation of electron cyclotron heated (ECH) heated plasmas.[28] This mechanism can enhance the effect of flow drive induced by ECH. For example, the ECH injection can induce a residual stress, Π^{Res} via conventional symmetry breaking mechanisms, and the flow gradient is thus enhanced by the negative viscosity increment resulting from dynamical symmetry breaking, i.e., $\langle v_\parallel\rangle' \sim \Pi^{\mathrm{Res}}/(\chi_\phi - |\chi_\phi^{\mathrm{Res}}|)$.

The dynamical symmetry breaking mechanism can be relevant to other types of turbulence, such as turbulence driven by ion temperature gradient (ITG). However, as only drift wave turbulence has been considered so far, the details of the ITG case are unknown at this stage. Its study is planned for a future publication. We conjecture that a qualitatively similar feedback mechanism may still work in ITG turbulence. This is because in ITG turbulence, the test flow shear enters the growth rate even without a frequency shift, and $\langle v_\parallel\rangle'$ enters via $k_\theta k_\parallel$ asymmetry. Further, for a kinetic theory of ITG instability, the basic non-adiabatic ion response is $\delta f \sim \{iL(\omega - \omega_{*,i})|e|\varphi/T_i\}f_0$, where L is a propagator. Hence, the frequency shift effect can enter here, as well. However, whether this will give a negative viscosity increment is unknown at this moment in time. We plan to address this question in a future publication, the preparation of which is ongoing.

In a similar vein, the mechanism proposed in this paper can be relevant to flow reversals during transition between linear Ohmic confinement (LOC) and saturated Ohmic confinement (SOC).[30] Intrinsic flow direction during the LOC-SOC transition can be set by geometrical symmetry breakers, e.g., $\langle v_E\rangle'$ and $I'(x)$. However, our mechanism enhances the flow profile gradient, via $\langle v_\parallel\rangle' \sim \Pi^{\mathrm{Res}}/(\chi_\phi - |\chi_\phi^{\mathrm{Res}}|)$. In LOC state, $\langle v_\parallel\rangle'$ is enhanced by $-|\chi_\phi^{\mathrm{Res}}|$ as a result of dynamical symmetry breaking. In SOC state, however, it is unclear about the effects on $\langle v_\parallel\rangle'$ by other types of turbulence, and this will be left for a future publication, as commented above.

The dynamical symmetry breaking is fundamentally different from the usual eddy tilting. In the dynamical symmetry breaking model, flow shear directly affects the linear growth rate by selecting some modes which grow faster, resulting in a spectral imbalance. Eddy tilting by $\langle v_\theta\rangle'$ in (r, θ) plane enters the correlator $\langle \tilde{v}_r \tilde{v}_\theta\rangle \sim \langle k_\theta k_r\rangle \sim -\langle k_\theta^2\rangle \langle v_\theta\rangle' \tau_c$, resulting in an unambiguous Reynolds work, and does not enter directly via stability. But in (r, z) plane, eddy tilting does not work, because $\partial_t k_z = -\partial_z(\omega + k_z\langle v_z\rangle) = 0$. In our case, the $\langle k_\theta k_r\rangle$ correlator couples differently to the growth rate, for different $\langle k_\theta k_r\rangle$. Thus, our mechanism is fundamentally different from eddy tilting.

ACKNOWLEDGMENTS

We are grateful to R. Hong, Y. Kosuga, A. Ashourvan, J. E. Rice, L. Cui, L. Wang, Ö. D. Gürcan, S. C. Thukar, and W. X. Wang for useful discussions. P. H. Diamond thanks participants in the 2013 and 2015 Festival de Théorie for many useful and interesting discussions. This work was supported by the U.S. Department of Energy, Office of Science, Office of Fusion Energy Sciences, under Award Nos. DE-FG02-04ER54738 and DE-AC52-07NA27344, and CMTFO Award No. DE-SC0008378.

[1]H. Reimerdes, T. C. Hender, S. A. Sabbagh, J. M. Bialek, M. S. Chu, A. M. Garofalo, M. P. Gryaznevich, D. F. Howell, G. L. Jackson, R. J. La Haye *et al.*, Phys. Plasmas **13**, 056107 (2006).
[2]S. D. Scott, P. H. Diamond, R. J. Fonck, R. J. Goldston, R. B. Howell, K. P. Jaehnig, G. Schilling, E. J. Synakowski, M. C. Zarnstorff, C. E. Bush *et al.*, Phys. Rev. Lett. **64**, 531 (1990).
[3]K. Ida, Y. Miura, T. Matsuda, K. Itoh, S. Hidekuma, and S.-I. Itoh (JFT-2M Group), Phys. Rev. Lett. **74**, 1990 (1995).
[4]J. Rice, W. Lee, E. Marmar, P. Bonoli, R. Granetz, M. Greenwald, A. Hubbard, I. Hutchinson, J. Irby, Y. Lin *et al.*, Nucl. Fusion **44**, 379 (2004).
[5]B. LaBombard, J. E. Rice, A. E. Hubbard, J. W. Hughes, M. Greenwald, R. S. Granetz, J. H. Irby, Y. Lin, B. Lipschultz, E. S. Marmar *et al.*, Phys. Plasmas **12**, 056111 (2005).
[6]P. H. Diamond, Y. Kosuga, Ö. D. Gürcan, C. J. McDevitt, T. Hahm, N. Fedorczak, J. E. Rice, W. X. Wang, S. Ku, J. M. Kwon *et al.*, Nucl. Fusion **53**, 104019 (2013).
[7]A. Peeters, C. Angioni, A. Bortolon, Y. Camenen, F. Casson, B. Duval, L. Fiederspiel, W. Hornsby, Y. Idomura, T. Hein *et al.*, Nucl. Fusion **51**, 094027 (2011).
[8]C. Angioni, Y. Camenen, F. Casson, E. Fable, R. McDermott, A. Peeters, and J. Rice, Nucl. Fusion **52**, 114003 (2012).

[9]Y. Kosuga, P. H. Diamond, and Ö. D. Gürcan, Phys. Plasmas **17**, 102313 (2010).
[10]Z. Yan, M. Xu, P. H. Diamond, C. Holland, S. H. Müller, G. R. Tynan, and J. H. Yu, Phys. Rev. Lett. **104**, 065002 (2010).
[11]N. Mattor and P. H. Diamond, Phys. Fluids **31**, 1180 (1988).
[12]A. L. Rogister, R. Singh, and P. K. Kaw, Phys. Plasmas **11**, 2106 (2004).
[13]P. Diamond, S. Itoh, K. Itoh, and T. Hahm, Plasma Phys. Controlled Fusion **47**, R35 (2005).
[14]Ö. D. Gürcan, P. Diamond, T. Hahm, and R. Singh, Phys. Plasmas **14**, 042306 (2007).
[15]Ö. D. Gürcan, P. H. Diamond, P. Hennequin, C. J. McDevitt, X. Garbet, and C. Bourdelle, Phys. Plasmas **17**, 112309 (2010).
[16]C. J. McDevitt, P. H. Diamond, Ö. D. Gürcan, and T. S. Hahm, Phys. Rev. Lett. **103**, 205003 (2009).
[17]Z. X. Lu, W. X. Wang, P. H. Diamond, G. Tynan, S. Ethier, C. Gao, and J. Rice, Phys. Plasmas **22**, 055705 (2015).
[18]J. E. Rice, Y. A. Podpaly, M. L. Reinke, R. Mumgaard, S. D. Scott, S. Shiraiwa, G. M. Wallace, B. Chouli, C. Fenzi-Bonizec, M. F. F. Nave *et al.*, Phys. Rev. Lett. **111**, 125003 (2013).
[19]S. Thakur, C. Brandt, L. Cui, J. Gosselin, A. Light, and G. Tynan, Plasma Sources Sci. Technol. **23**, 044006 (2014).
[20]L. Cui, A. Ashourvan, S. C. Thakur, R. Hong, P. Diamond, and G. R. Tynan, Phys. Plasmas **23**, 055704 (2016).
[21]R. Hong, J. C. Li, S. C. Thakur, P. H. Diamond, and G. R. Tynan, in 2016 U.S. Transport Task Force Workshop, Denver, CO, 2016.
[22]J. Abiteboul, P. Ghendrih, V. Grandgirard, T. Cartier-Michaud, G. Dif-Pradalier, X. Garbet, G. Latu, C. Passeron, Y. Sarazin, A. Strugarek *et al.*, Plasma Phys. Controlled Fusion **55**, 074001 (2013).
[23]P. Mantica, C. Angioni, C. Challis, G. Colyer, L. Frassinetti, N. Hawkes, T. Johnson, M. Tsalas, P. C. deVries, J. Weiland *et al.*, Phys. Rev. Lett. **107**, 135004 (2011).
[24]P. C. de Vries, K. M. Rantamki, C. Giroud, E. Asp, G. Corrigan, A. Eriksson, M. de Greef, I. Jenkins, H. C. M. Knoops, P. Mantica *et al.*, Plasma Phys. Controlled Fusion **48**, 1693 (2006).
[25]L. Wang, P. H. Diamond, and T. S. Hahm, Plasma Phys. Controlled Fusion **54**, 095015 (2012).
[26]X. Garbet, C. Bourdelle, G. T. Hoang, P. Maget, S. Benkadda, P. Beyer, C. Figarella, I. Voitsekovitch, O. Agullo, and N. Bian, Phys. Plasmas **8**, 2793 (2001).
[27]X. Garbet, Y. Sarazin, P. Ghendrih, S. Benkadda, P. Beyer, C. Figarella, and I. Voitsekhovitch, Phys. Plasmas **9**, 3893 (2002).
[28]Y. Shi, W. Ko, J. Kwon, P. Diamond, S. Lee, S. Ko, L. Wang, S. Yi, K. Ida, L. Terzolo *et al.*, Nucl. Fusion **53**, 113031 (2013).
[29]R. M. McDermott, C. Angioni, R. Dux, A. Gude, T. Ptterich, F. Ryter, G. Tardini, and ASDEX Upgrade Team, Plasma Phys. Controlled Fusion **53**, 035007 (2011).
[30]J. E. Rice, I. Cziegler, P. H. Diamond, B. P. Duval, Y. A. Podpaly, M. L. Reinke, P. C. Ennever, M. J. Greenwald, J. W. Hughes, Y. Ma *et al.*, Phys. Rev. Lett. **107**, 265001 (2011).